The effect of iridium(III) ions on the formation of iron oxides in a highly alkaline medium

Stjepko Krehula *, Svetozar Musić

Division of Materials Chemistry, Ruđer Bošković Institute, PO Box 180, HR-10002 Zagreb, Croatia

ARTICLE INFO

ABSTRACT

The effect of the presence of Ir^{3+} ions on the formation of iron oxides in a highly alkaline precipitation system was investigated using X-ray powder diffraction (XRD), [57]Fe Mössbauer and FT-IR spectroscopies, field emission scanning electron microscopy (FE-SEM) and energy dispersive X-ray spectroscopy (EDS). Monodispersed lath-like α-FeOOH (goethite) particles precipitated by hydrothermal treatment in a highly alkaline medium with the addition of tetramethylammonium hydroxide (TMAH) were used as reference material. The presence of Ir^{3+} ions in the precipitation system strongly influenced the phase composition, magnetic, structural and morphological properties of obtained samples. The formation of α-Fe$_2$O$_3$ (hematite) along with α-FeOOH in the first stage of hydrothermal treatment and the transformation of α-FeOOH and α-Fe$_2$O$_3$ to Fe$_3$O$_4$ (magnetite) by a longer hydrothermal treatment was caused by the presence of Ir^{3+} ions. Ir^{3+} for Fe^{3+} substitution in the structure of α-FeOOH brought about changes in unit-cell dimensions, crystallinity, particle size and shape, hyperfine magnetic field and infrared bands positions. Ir^{3+} for Fe^{3+} substitution in the structure of α-Fe$_2$O$_3$ led to an increase in the temperature of the Morin transition; Mössbauer spectroscopy showed the presence of α-Fe$_2$O$_3$ in the antiferromagnetically ordered state at 293 K.

1. Introduction

Iron oxides are common and widespread compounds that play an important role in many natural processes [1]. They are also valuable materials for various technological applications (pigments, magnetic recording devices, ferrofluids, catalysts, adsorbents, abrasives, gas sensors, various biomedical applications, etc.) [1–8]. The application of iron oxides demands well defined specific properties (magnetic, electric, catalytic, adsorption, thermal, etc.). These properties are dependent on the size and shape of iron oxide particles, as well as on the content of various foreign metal cations incorporated into the structure of a particular iron oxide [1,2,9–15].

A common method used in the laboratory synthesis of iron oxides is precipitation from iron(III) and iron(II) salt solutions. Along with the type of iron salt, concentration of iron ions, pH, temperature, aging time and the presence of additives (various ligands and anions), the presence of foreign metal cations is also an important factor influencing the microstructural properties of iron oxides thus prepared [1,16]. In our previous works we investigated the influence of some foreign metal cations during the precipitation of monodispersed lath-like α-FeOOH nanoparticles in a highly

alkaline medium on the final products properties and we observed a strong influence of these cations on the phase composition and microstructural properties of obtained products [17–20].

Precipitation of iron oxides in the presence of iridium ions has been poorly investigated, in spite of the significant potential of Ir^{3+}-for-Fe^{3+} substitution (the same cationic charge and similar radii). A limited number of articles has been published on the subject of Fe–Ir mixed oxides. Liu [21] investigated the magnetic properties of hematite doped with Ir^{4+} ions and observed an abrupt increase in the Morin transition temperature even for small iridium substitutions. Punnoose et al. [22] investigated the magnetic properties of ferrihydrite nanoparticles doped with Ir and concluded that Ir-for-Fe substitution occurs primarily at the surface of ferrihydrite nanoparticles. Using [57]Fe Mössbauer spectroscopy, Berry et al. [23,24] investigated titania-supported iron(III)–iridium(III) catalysts. By means of different impregnation sequences Zhang et al. [25] prepared the IrFeO$_x$/SiO$_2$ catalyst which was very active and selective for preferential oxidation of CO under a H$_2$-rich atmosphere. Hematite with surface-deposited IrO$_2$ particles showed promising results as a catalyst for light-induced water splitting [26].

According to the best of our knowledge, no systematic study of the influence of iridium ions on the formation of iron oxides has been published yet. In the present work we have studied the influence of the presence of Ir^{3+} ions on the precipitation of iron oxides in a highly alkaline medium. The uniform lath-like α-FeOOH

* Corresponding author. Tel.: +385 1 4561 094; fax: +385 1 4680 098.
E-mail address: krehul@irb.hr (S. Krehula).
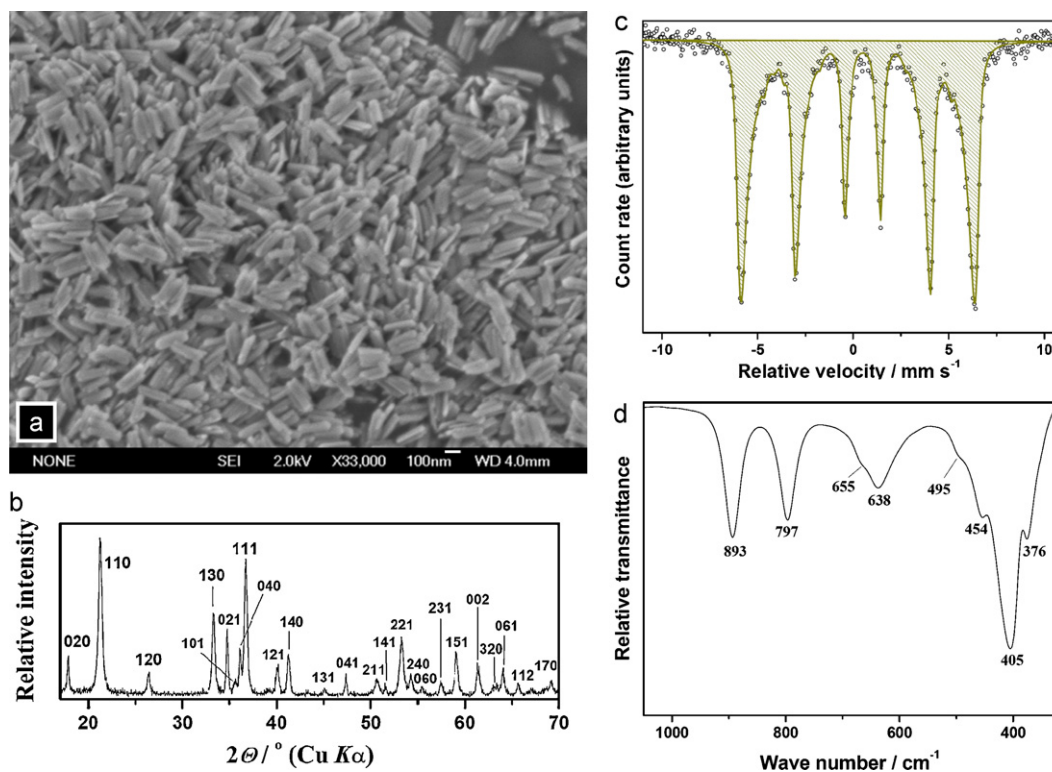
Fig. 1. Reference sample G-2 h: (a) FE-SEM image, (b) X-ray powder diffraction pattern, (c) ^{57}Fe Mössbauer spectrum (recorded at 20 °C), and (d) a characteristic part of the FT-IR spectrum.

particles (Fig. 1) prepared in our earlier work [27,28] were used as reference material.

2. Experimental

2.1. Preparation of samples

Iron(III) chloride hexahydrate (FeCl$_3$ 6H$_2$O) of analytical purity, supplied by *Kemika*, iridium(III) chloride (IrCl$_3$) and a tetramethylammonium hydroxide (TMAH) solution (25%, w/w, electronic grade 99.9999%), both supplied by *Alfa Aesar*®, were used. Twice-distilled water prepared in our own laboratory was used in all experiments. Predetermined volumes of FeCl$_3$ and IrCl$_3$ solutions and twice-distilled water were mixed, then TMAH was added as a precipitating agent. The exact experimental conditions for sample preparation are given in Table 1. Thus formed aqueous suspensions were vigorously shaken for ~10 min, then heated at 160 °C, using the Parr general-purpose bomb (model 4744) comprising a Teflon vessel and a cup. After the proper heating time the precipitates were cooled to room temperature (the mother liquor pH ≈13.5) and subsequently washed with twice-distilled water to remove "neutral electrolyte". The ultraspeed *Sorvall* RC2-B centrifuge was used for the separation of solid and liquid components. The solid precipitates were dried one day at 60 °C. After drying all precipitates were characterized by X-ray powder diffraction, Mössbauer and FT-IR spectroscopies, as well as high-resolution scanning electron microscopy and energy dispersive X-ray spectroscopy.

2.2. Instrumentation

^{57}Fe Mössbauer spectra were recorded at 20 °C (293 K) in the transmission mode using a standard *WissEl* (Starnberg, Germany) instrumental configuration. A ^{57}Co/Rh Mössbauer source was used. The velocity scale and all data refer to the metallic α-Fe absorber at 20 °C. A quantitative analysis of the recorded spectra was made using the *MossWinn* program.

X-ray powder diffractometer APD 2000 (CuKα radiation, graphite monochromator, NaI-Tl detector) manufactured by *ItalStructures* (Riva Del Garda, Italy) was used. The selected samples were mixed with about 10% KBr (for IR-spectroscopy, supplied by *Fluka*) as an internal standard. The exact positions and full width at half maximum (FWHM) values of the diffraction lines were obtained by fitting a pseudo-Voigt function to experimental data using the *WinDust32* program (*ItalStructures*). The unit cell dimensions of α-FeOOH and α-(Fe,Ir)OOH were calculated from the positions of lines (0 2 0), (1 1 0), (1 2 0), (1 3 0), (0 2 1), (1 1 1), and (1 4 0) using the *XLAT* least squares program [29].

Table 1
Concentration conditions for the preparation of samples by autoclaving at 160 °C and the phase composition of solid samples determined by X-ray powder diffraction.

Sample	[FeCl$_3$] (mol dm^{-3})	[IrCl$_3$] (mol dm^{-3})	100 [Ir]/([Ir] + [Fe])	TMAH[a] (mol dm^{-3})	Aging time/h	Phase composition[b]
G-2 h	0.1	0	0	0.7	2	G
IrG1-2 h	0.1	1.01×10^{-3}	1	0.7	2	G
IrG1-6 h	0.1	1.01×10^{-3}	1	0.7	6	G
IrG1-24 h	0.1	1.01×10^{-3}	1	0.7	24	G + H + M
IrG1-72 h	0.1	1.01×10^{-3}	1	0.7	72	M + H
IrG5-2 h	0.1	5.27×10^{-3}	5	0.7	2	G + H
IrG5-6 h	0.1	5.27×10^{-3}	5	0.7	6	G + H
IrG5-24 h	0.1	5.27×10^{-3}	5	0.7	24	H + G + M
IrG5-72 h	0.1	5.27×10^{-3}	5	0.7	72	M + Ir
IrG10-2 h	0.1	1.11×10^{-2}	10	0.7	2	G + H
IrG10-6 h	0.1	1.11×10^{-2}	10	0.7	6	G + H
IrG10-24 h	0.1	1.11×10^{-2}	10	0.7	24	M + H + G
IrG10-66 h	0.1	1.11×10^{-2}	10	0.7	66	M + Ir

[a] TMAH: tetramethylammonium hydroxide (25%, w/w).
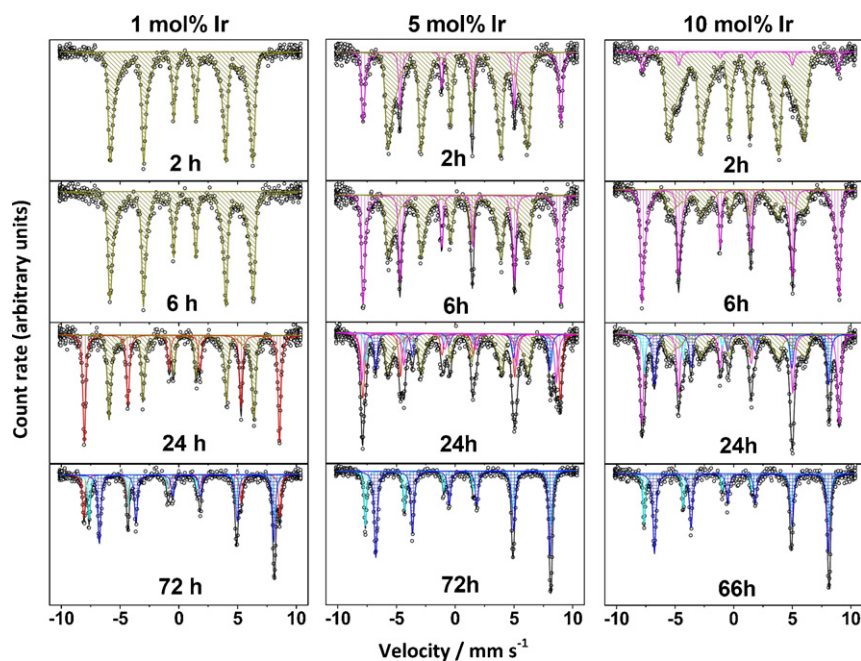[b] G: goethite (α-FeOOH); H: hematite (α-Fe$_2$O$_3$); M: magnetite (Fe$_3$O$_4$).

Fig. 2. ^{57}Fe Mössbauer spectra (recorded at 20 °C) of samples obtained after various hydrothermal treatment times in the presence of 1, 5 or 10 mol% of Ir^{3+} ions.

Fourier transform infrared (FT-IR) spectra were recorded at RT using a *Perkin-Elmer* spectrometer (model 2000). The FT-IR spectrometer was connected to a PC with the installed IRDM (IR data manager) program to process the recorded spectra. The specimens were pressed into small discs using a spectroscopically pure KBr matrix.

A thermal field emission scanning electron microscope (FE-SEM, model JSM-7000F, manufactured by *JEOL Ltd.*) was used. FE-SEM was linked to the EDS/INCA 350 (energy dispersive X-ray analyser) manufactured by *Oxford Instruments Ltd.*. The specimens were not coated with an electrically conductive surface layer.

3. Results and discussion

### 3.1. ^{57}Fe Mössbauer spectroscopy

The Mössbauer spectra of synthesized samples are shown in Fig. 2, while the calculated Mössbauer parameters and phase identification are given in Table 2. The sextet corresponding to α-FeOOH

Table 2
^{57}Fe Mössbauer parameters at 20 °C calculated for synthesized samples and phase identification.

Sample	Spectral line	δ (mm s^{-1})	2ε (mm s^{-1})	B_{hf}[a] (T)	Γ (mm s^{-1})	Area (%)	Phase
G-2 h	M	0.37	−0.26	35.7 (38.2)	0.24	100	α-FeOOH
IrG1-2 h	M	0.37	−0.27	35.4 (37.5)	0.25	100	α-(Fe,Ir)OOH
IrG1-6 h	M	0.37	−0.26	36.0 (38.0)	0.24	100	α-(Fe,Ir)OOH
IrG1-24 h	M	0.37	−0.27	36.7 (38.4)	0.24	53.1	α-(Fe,Ir)OOH
	M	0.37	−0.22	51.5	0.27	46.9	α-Fe$_2$O$_3$
IrG1-72 h	M	0.36	−0.20	51.7	0.27	27.1	α-Fe$_2$O$_3$
	M	0.27	−0.01	49.1	0.23	24.7	Fe$_3$O$_4$ (tet)
	M	0.66	0.00	46.1	0.29	48.2	Fe$_3$O$_4$ (oct)
IrG5-2 h	M	0.37	−0.27	34.2 (37.0)	0.27	76.8	α-(Fe,Ir)OOH
	M	0.38	0.41	51.9 (52.4)	0.22	23.2	α-(Fe,Ir)$_2$O$_3$
IrG5-6 h	M	0.37	−0.26	34.2 (37.0)	0.29	56.4	α-(Fe,Ir)OOH
	M	0.37	0.41	51.7 (52.2)	0.22	43.6	α-(Fe,Ir)$_2$O$_3$
IrG5-24 h	M	0.37	−0.27	34.2 (37.0)	0.26	33.4	α-(Fe,Ir)OOH
	M	0.37	0.35	52.1	0.32	24.2	α-(Fe,Ir)$_2$O$_3$
	M	0.38	−0.09	51.4	0.36	20.1	α-(Fe,Ir)$_2$O$_3$
	M	0.29	0.04	49.1	0.25	8.4	Fe$_3$O$_4$ (tet)
	M	0.65	0.00	46.0	0.33	13.9	Fe$_3$O$_4$ (oct)
IrG5-72 h	M	0.27	0.00	49.1	0.24	33.3	Fe$_3$O$_4$ (tet)
	M	0.66	0.00	46.1	0.31	66.7	Fe$_3$O$_4$ (oct)
IrG10-2 h	M	0.37	−0.27	32.7 (36.5)	0.26	92.4	α-(Fe,Ir)OOH
	M	0.37	0.42	51.8	0.38	7.6	α-(Fe,Ir)$_2$O$_3$
IrG10-6 h	M	0.37	−0.27	32.3 (36.0)	0.26	35.1	α-(Fe,Ir)OOH
	M	0.37	0.42	51.3 (52.2)	0.21	64.9	α-(Fe,Ir)$_2$O$_3$
IrG10-24 h	M	0.37	−0.27	32.7 (36.5)	0.26	28.1	α-(Fe,Ir)OOH
	M	0.37	0.41	52.2	0.34	36.2	α-(Fe,Ir)$_2$O$_3$
	M	0.28	0.02	49.0	0.30	14.1	Fe$_3$O$_4$ (tet)
	M	0.66	0.00	46.1	0.36	21.6	Fe$_3$O$_4$ (oct)
IrG10-66 h	M	0.27	0.00	49.1	0.23	32.4	Fe$_3$O$_4$ (tet)
	M	0.66	0.01	46.1	0.30	67.6	Fe$_3$O$_4$ (oct)

Errors: $\delta = \pm 0.01$ mm s^{-1}, $2\varepsilon = \pm 0.01$ mm s^{-1}, $B_{hf} = \pm 0.2$ T, $\Gamma = \pm 0.01$ mm s^{-1}. Isomer shift is given relative to α-Fe.

[a] Two values of B_{hf} are given for the spectra fitted by distribution of HMF: average B_{hf} (first value) and the most probable B_{hf} (in parenthesis).
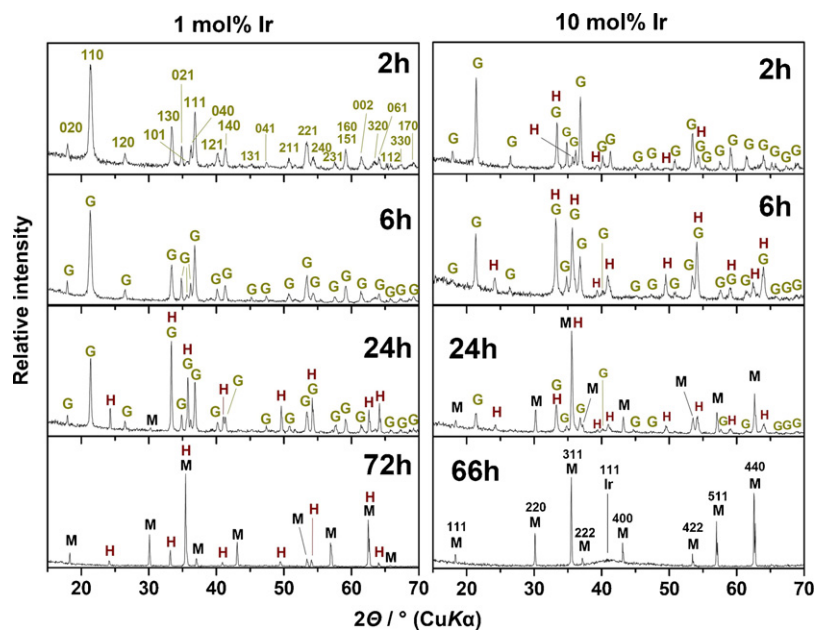
Fig. 3. XRD patterns (recorded at 20 °C) of samples obtained after various hydrothermal treatment times in the presence of 1 or 10 mol% of Ir^{3+} ions (G: α-FeOOH; H: α-Fe$_2$O$_3$; M: Fe$_3$O$_4$; and Ir: Iridium).

in the Mössbauer spectra of obtained samples was fitted taking into account the hyperfine magnetic field (HMF) distribution in the range from 20 to 40 T. The spectra of the samples obtained after 2 and 6 h of hydrothermal treatment in the presence of 1 mol% of Ir^{3+} ions (samples IrG1-2 h and IrG1-6 h) consisted of a typical asymmetric sextet corresponding to α-FeOOH of medium crystallinity [30], similar to the spectrum of reference sample G-2 h (Fig. 1c). Line intensities in these α-FeOOH sextets deviate from the theoretical ratio 3:2:1:1:2:3 more than the sextet of reference α-FeOOH sample (3:2.1:1:1:2.1:3 for sample G-2 h, 3:2.3:1:1:2.3:3 for IrG1-2 h and 3:2.5:1:1:2.5:3 for IrG1-6 h) due to a somewhat preferred orientation of lath-like α-FeOOH particles in powder samples with b- and c-crystallographic axes perpendicular to the direction of γ-rays. The presence of 1 mol% of Ir^{3+} ions in the precipitation system (sample IrG1-2 h) led to a slight decrease in the HMF of the formed α-FeOOH in comparison with reference sample G-2 h (Table 2). This reduction can be attributed to the effect of Fe^{3+} by Ir^{3+} substitution in the structure of α-FeOOH, so the chemical formula of this solid solution compound can be written out as α-(Fe,Ir)OOH. HMF values for sample IrG1-6 h (Table 2) were increased due to improved α-(Fe,Ir)OOH crystallinity. However, these values were somewhat lower in comparison with the HMF in a pure α-FeOOH sample formed in identical conditions [28] due to the effect of substituted Ir^{3+} ions. Two sextets in the Mössbauer spectrum of sample obtained after 24 h of hydrothermal treatment (IrG1-24 h) correspond to α-(Fe,Ir)OOH and weakly ferromagnetic α-Fe$_2$O$_3$. A relatively high value of HMF (51.5 T) and the maintenance of magnetic order as in pure α-Fe$_2$O$_3$ do not indicate any significant Ir-for-Fe substitution in the α-Fe$_2$O$_3$ structure. Further hydrothermal treatment (72 h) resulted in a complete disappearance of α-(Fe,Ir)OOH and a partial transformation of α-Fe$_2$O$_3$ to Fe$_3$O$_4$ by the reduction of Fe(III)–Fe(II) with TMAH thermal decomposition products and iridium as a catalyst.

The presence of a higher concentration of Ir^{3+} ions in the precipitation system (5 mol%) led to the formation of α-Fe$_2$O$_3$ besides α-(Fe,Ir)OOH after only 2 h of hydrothermal treatment. Thus formed α-Fe$_2$O$_3$ has a distinct Mössbauer spectrum in comparison with pure (undoped) α-Fe$_2$O$_3$. The Mössbauer spectrum

(recorded at 293 K) of sample IrG5-2 h (Fig. 2) along with corresponding parameters obtained by fitting (Table 2) showed the presence of α-Fe$_2$O$_3$ in the antiferromagnetically ordered state, unlike the pure, undoped α-Fe$_2$O$_3$ which is in the weakly ferromagnetic state at room temperature. Such a change in the magnetic order indicates a significant Ir^{3+} for Fe^{3+} substitution, so this phase can be written out as α-(Fe,Ir)$_2$O$_3$. The Ir^{3+} for Fe^{3+} substitution in the α-Fe$_2$O$_3$ structure was responsible for an increase in the temperature of the Morin transition, i.e., a change in the room temperature magnetic order of this phase.

The Morin transition is a change in the magnetic state of hematite at a temperature of about 260 K (for the samples of good crystallinity) [31–34]. The magnetic spins of Fe^{3+} cations are oriented antiparallel in the [0 0 1] direction (antiferromagnetic state) at temperatures below ∼260 K (Morin transition temperature, T_M) and almost antiparallel (with a minor spin canting) in the plane perpendicular to the [0 0 1] direction (weakly ferromagnetic state) at temperatures above T_M and below Curie temperature ($T_C \approx 955$ K). Mössbauer spectroscopy is one of the best techniques for distinguishing these two types of magnetic ordering and for determining the Morin transition temperature. Incorporation of various metal cations into the structure of α-Fe$_2$O$_3$ strongly affected the Morin transition temperature [34]. The majority of incorporated cations reduced or suppressed this transition [35–40] (down to liquid helium temperature), while a few of them (Rh^{3+}, Ru^{3+}, Ir^{4+}), on the other hand, caused an increase in T_M [21,41–43]. This effect has been largely explained by an increase in the single-ion magnetic anisotropy component in hematite as a result of strong anisotropy cations Rh^{3+}, Ru^{3+} or Ir^{4+} incorporated. In the present work we observed by Mössbauer spectroscopy the antiferromagnetic order in the Ir^{3+}-doped hematite at 293 K and in this way clearly demonstrated the effect of the incorporation of this cation in hematite on the increase in the Morin transition temperature.

The Mössbauer spectrum of sample IrG5-6 h (Fig. 2) shows an increase in the quantity of antiferromagnetic α-(Fe,Ir)$_2$O$_3$ relative to α-(Fe,Ir)OOH with the aging of the precipitation system. However, a hydrothermal treatment of the system with 5 mol% of Ir^{3+} ions for 24 h results in a partial transformation of α-(Fe,Ir)OOH

and antiferromagnetic α-(Fe,Ir)$_2$O$_3$ to ferromagnetic α-Fe$_2$O$_3$ and Fe$_3$O$_4$ (Fig. 2, Table 2). A longer hydrothermal treatment (72 h, Fig. 2) resulted in the complete transformation of α-(Fe,Ir)OOH and α-(Fe,Ir)$_2$O$_3$ to stoichiometric Fe$_3$O$_4$ (octahedral Fe$^{2.5+}$:tetrahedral Fe^{3+} = 2:1) (Table 2).

Similar to the case of samples obtained in the presence of 5 mol% of Ir^{3+} ions, the presence of 10 mol% of Ir^{3+} resulted in a gradual transformation of α-(Fe,Ir)OOH to antiferromagnetic α-(Fe,Ir)$_2$O$_3$ (2 and 6 h of aging) followed by the formation of Fe$_3$O$_4$, after a sufficient aging time (Fig. 2, Table 2).

3.2. X-ray powder diffraction

Crystalline phases in synthesized samples (Table 1) were determined from the recorded XRD patterns (Fig. 3) using JCPDS PDF cards No. 29-713 for α-FeOOH, No. 33-664 for α-Fe$_2$O$_3$, No. 19-629 for Fe$_3$O$_4$ and No. 06-0598 for iridium. Unit cell parameters of α-FeOOH and α-(Fe,Ir)OOH, calculated from the positions of the corresponding diffraction lines, and the FWHM values of the strongest diffraction lines for samples G-2 h, IrG1-2 h, IrG5-2 h and IrG10-2 h are given in Table 3. Molar fractions of iridium cations were given as molar fractions in the initial solutions (nominal) and molar fractions in the powder samples as determined by EDS. Decrease in the iridium content in powder samples in comparison with initial systems indicates a partial loss of Ir^{3+} ions during sample washing.

Phase identification confirmed the results of Mössbauer spectroscopy measurements. Only the α-FeOOH diffraction lines were present in the patterns of samples IrG1-2 h and IrG6-2 h. Further hydrothermal treatment led to a gradual transformation of α-FeOOH to α-Fe$_2$O$_3$, followed by the reduction of Fe(III)–Fe(II) with TMAH thermal decomposition products (such as methanol and trimethylamine [44]) in the presence of iridium as a catalyst. The presence of α-Fe$_2$O$_3$ diffraction lines in the pattern of the sample obtained after 72 h of treatment indicated an unfinished α-Fe$_2$O$_3 \rightarrow$ Fe$_3$O$_4$ transformation. The XRD patterns of samples prepared in the presence of 10 mol% of Ir(III) ions showed the presence of α-Fe$_2$O$_3$ only after 2 h of hydrothermal treatment and faster transformation α-FeOOH $\rightarrow \alpha$-Fe$_2$O$_3 \rightarrow$ Fe$_3$O$_4$. This transformation was completed in the sample obtained after 66 h of treatment; strong and narrow Fe$_3$O$_4$ diffraction lines emerged, accompanied by broad lines of nanosize metallic iridium (Fig. 4a) [45].

In our previous studies [17–20,46–49] we have investigated the influence of various metal cations on the formation of iron oxides in a highly alkaline medium in the presence of TMAH. Formation of Fe$_3$O$_4$ has been observed only in the case of the platinum group metal cations (ruthenium, palladium, platinum and rhodium) [18,46–49], well known for their excellent catalytic properties. In the absence of the platinum group metal ions Fe^{3+} ions have not been reduced and only Fe(III) oxides have been formed [17,19,20,27,28]. On the other hand, in the presence of even a small amount (1 mol% or less) of platinum group metal ions α-FeOOH has been completely transformed to Fe$_3$O$_4$ [18,46–49]. On the basis of these observations, it can be concluded that the platinum group metals act as catalysts for the transformation α-FeOOH $\rightarrow$ Fe$_3$O$_4$ in the presence of TMAH. In the present case, decomposition products of TMAH (such as CH$_3$OH) and iridium nanoparticles play an important role in this transformation.

A study of the influence of Ir^{3+} ions on the α-FeOOH unit-cell parameters (Fig. 4b, Table 3) clearly showed that the unit-cell parameter a was decreased and the unit-cell parameter b was increased with an increase in the concentration of Ir^{3+} ions. At the same time, the unit-cell parameter c remained unchanged. Although the Ir-for-Fe substitution in α-FeOOH, to the best of our knowledge, has not been studied yet, similar changes of unit-cell parameters were observed for some other cations. Zn^{2+} and Cu^{2+}
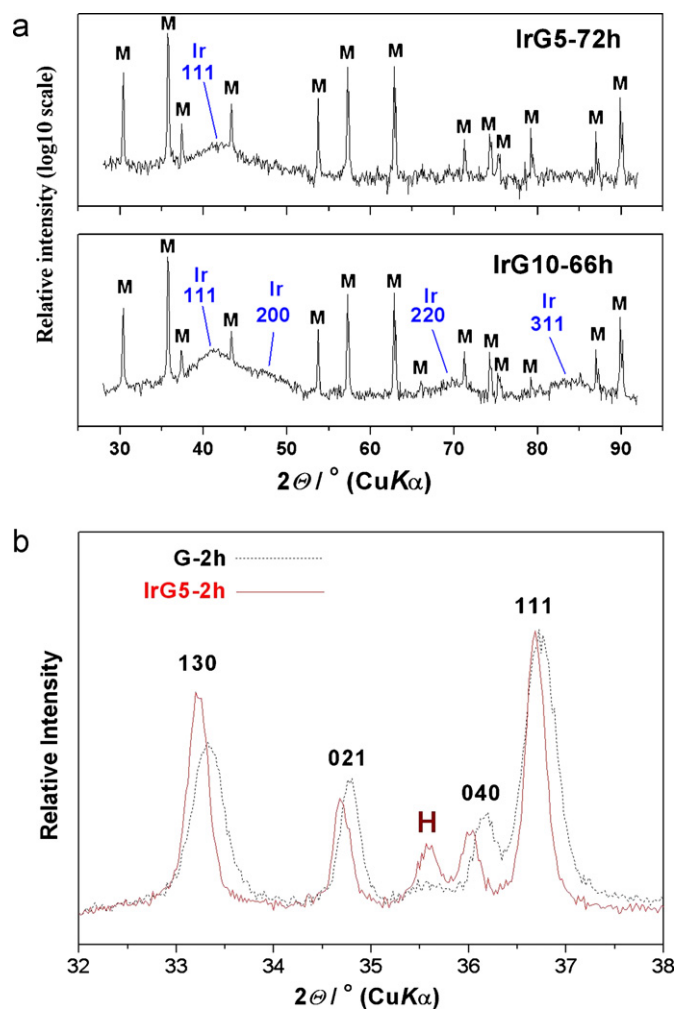

Fig. 4. (a) XRD patterns of samples IrG5-72 h and IrG10 in the 2Θ range from 28° to 92° with intensity presented in logarithmic scale (M: Fe$_3$O$_4$; Ir: iridium). (b) A characteristic part of XRD patterns of reference sample (G-2 h) and sample obtained under the same conditions in the presence of 5 mol% of Ir^{3+} ions (IrG5-2 h). The effect of Ir^{3+} ions on the shift in the positions and the decrease in the width of α-FeOOH diffraction lines is clearly visible (H: α-Fe$_2$O$_3$).

incorporation into α-FeOOH [50] also caused an increase in b, a decrease in a and constancy in parameter c. Increase in b and decrease in a was also observed for Mn^{3+} incorporation, but in this case parameter c was decreased [51–53].

The incorporation of Ir^{3+} ions into α-FeOOH led to the narrowing of diffraction lines (Fig. 4b, Table 3) which indicated an increase in the size of crystalline domains. A similar effect was observed in the case of incorporated Mn^{3+} ions [51]. This effect can be attributed to the formation of less α-FeOOH nuclei (relative to the reference system) in the nucleation stage of precipitation due to the presence of Ir^{3+} ions which led to the growth of larger α-FeOOH crystals in the subsequent stages of crystallization.

3.3. FT-IR spectroscopy

The FT-IR spectrum of reference sample G-2 h in the wave number range from 1000 to 300 cm^{-1} is shown in Fig. 1d. The IR bands at 893 and 797 cm^{-1} correspond to Fe—O—H bending vibrations, whereas the bands at lower wave numbers correspond to Fe—O and Fe—OH stretching vibrations or crystal lattice vibrations [54–56]. The two most intense of these lattice vibration bands (LVB) at 638

Table 3
Unit cell parameters and FWHM values of the strongest diffraction lines for pure and Ir-substituted α-FeOOH phase in the selected samples.

| Sample	100·[Ir]/([Ir]+[Fe])		Unit cell parameter/Å			$V/\text{Å}^3$	FWHM (°2Θ)			
	Nominal	By EDS	a	b	c		(1 1 0)	(1 3 0)	(0 2 1)	(1 1 1)
G-2 h	0	0	4.613(1)	9.955(3)	3.023(0)	138.8(1)	0.478	0.363	0.219	0.350
IrG1-2 h	1	0.57	4.611(0)	9.960(2)	3.023(0)	138.8(1)	0.444	0.317	0.176	0.306
IrG5-2 h	5	2.50	4.607(1)	9.979(2)	3.023(0)	139.0(1)	0.213	0.217	0.139	0.195
IrG10-2 h	10	4.32	4.605(1)	9.984(5)	3.023(0)	139.0(1)	0.215	0.210	0.141	0.193

and 405 cm^{-1} corresponds to the lattice vibrations with a transition moment parallel to the a-axis (LVB$_a$) and c-axis (LVB$_c$), respectively [55,56].

The presence of Ir^{3+} ions significantly affected the positions of α-FeOOH infrared bands (Fig. 5). Fe—O—H bending vibration bands were slightly shifted to lower wavenumbers in the sample synthesized at 1 mol% of Ir^{3+} ions (sample IrG1-2 h). However, in the presence of higher amounts of Ir^{3+} ions (5 and 10 mol%) these bands were shifted to higher wavenumbers (samples IrG5-2 h and IrG10-2 h). These opposite shifts can be attributed to the sum of factors with a varying influence on the vibrational modes, such as changes in the hydrogen bond strength, atomic positions and bond angles due to Ir-for-Fe substitution, as well as a change in the strength of the OH···O hydrogen bond resulting from a change in the crystallinity of samples [27,28,56]. The aging of samples led to a shift of these bands to higher values for all concentrations of Ir^{3+} ions due to an increase in the strength of the hydrogen bond caused by improved crystallinity of α-FeOOH in these samples [56,57].

The infrared bands corresponding to lattice vibrations also showed opposite shifts for lower and higher concentrations of Ir^{3+} ions. The shifts in the position of LVB$_a$ from 638 cm^{-1} in the spectrum of reference sample G to 641 and 627 cm^{-1} in the spectra of samples IrG1-2 h and IrG5-2 h, respectively, correspond to a combination of various effects, such as Ir-for-Fe substitution in the structure of α-FeOOH and changes in the shape of particles [20,28,55,56]. For the same reasons LVB$_c$ was shifted from 407 cm^{-1} (sample G) to 399 cm^{-1} (sample IrG1-2 h), 414 cm^{-1} (sample IrG5-2 h) or 411 cm^{-1} (sample IrG10-2 h). The positions of LVBs depend on the shape of particles, i.e., on the ratio between the particle size along the a- and c-axes (d_a/d_c). α-FeOOH particles in sample IrG1-2 h (see Section 3.4, Fig. 6a and b) were slightly thicker (a-axis direction) and wider (b-axis direction), but significantly longer (c-axis direction) in comparison with reference sample G (Fig. 1a). The particle size ratio in the a- and c-axes direction was decreased and, consequently, LVB$_a$ was shifted to a higher and LVB$_c$ to a lower wavenumber. However, α-FeOOH particles in samples IrG5-2 h (see Section 3.4, Fig. 7a) were significantly thicker, wider
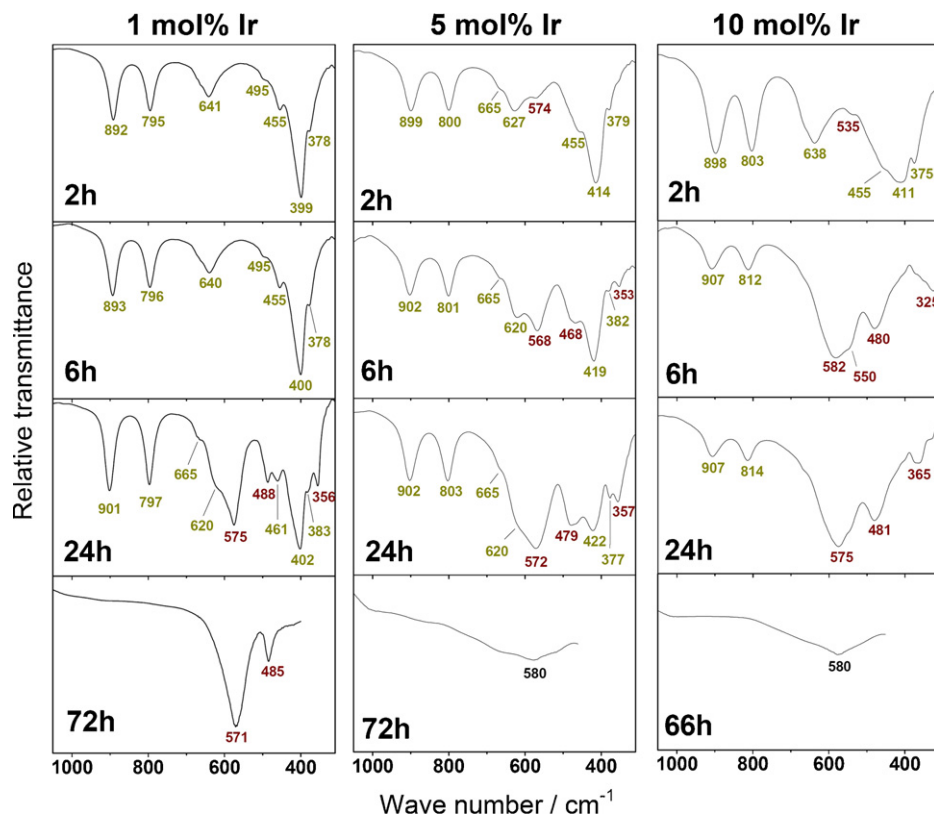
Fig. 5. The FT-IR spectra of samples obtained after various hydrothermal treatment times in the presence of 1, 5 or 10 mol% of Ir^{3+} ions.
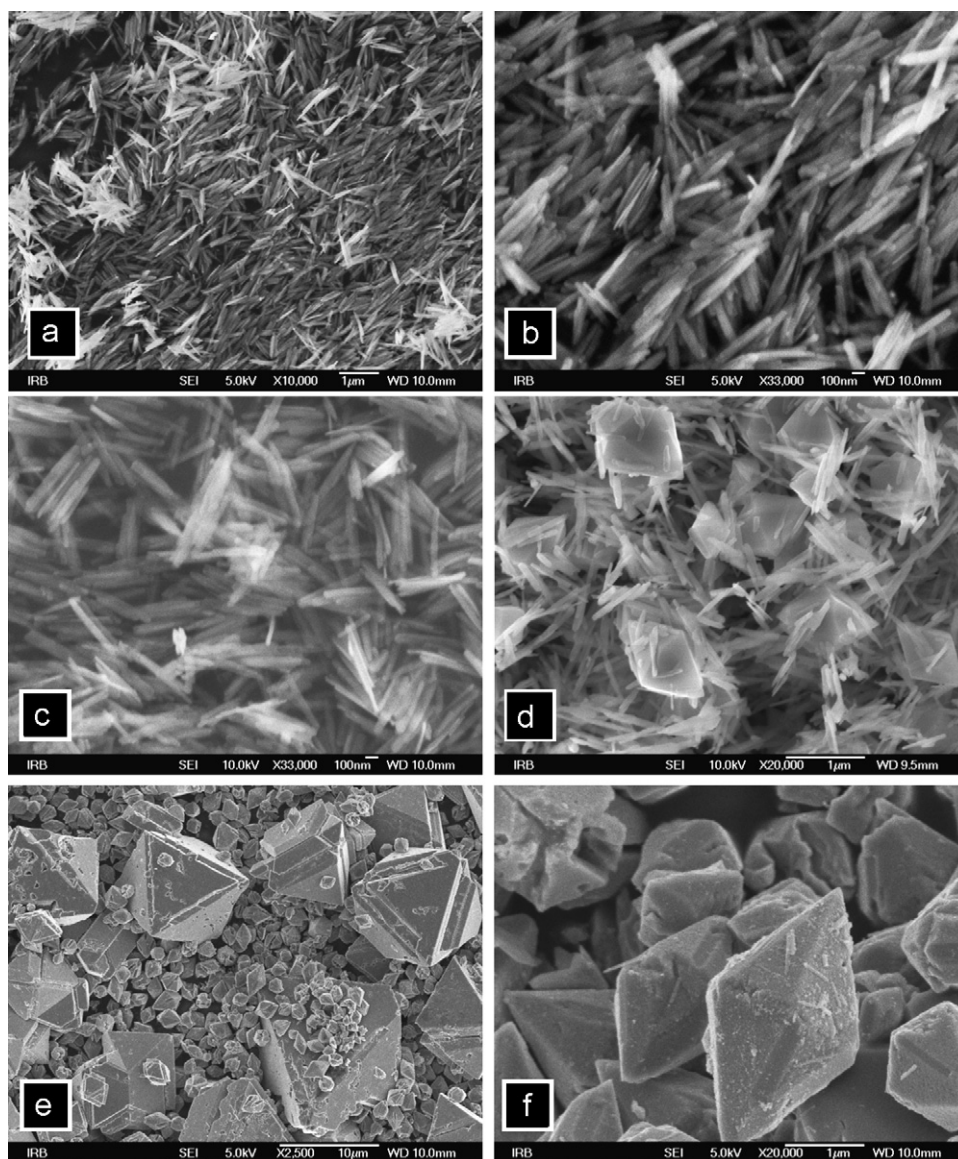
Fig. 6. FE-SEM images of samples: IrG1-2 h at lower (a) and higher (b) magnification, IrG1-6 h (c), IrG1-24 h (d), IrG1-72 h at lower (e) and higher (f) magnification.

and longer in comparison with reference sample G. In this case, the ratio of particle sizes in the a- and c-axes direction (d_a/d_c) was increased and, consequently, LVB_a was shifted to a lower and LVB_c to a higher wavenumber. The aging of samples influenced the shifts of LVB_a to lower and those of LVB_c to higher values for all concentrations of Ir^{3+} ions due to changes in the shape of α-FeOOH particles (d_a/d_c ratio is increased) and improvement in the crystallinity.

The presence of α-Fe_2O_3 in samples IrG1-24 h, Irg1-72 h, IrG5-2 h, IrG5-6 h, IrG5-24 h, IrG10-6 h and IrG10-24 h was confirmed on the basis of strong bands at about 570 and 480 cm^{-1}. The infrared spectrum of α-Fe_2O_3 depends on the shape of particles [58,59] and the positions of these bands match closely those in the spectra of pseudocubic α-Fe_2O_3 particles [59–61], which is in line with the FE-SEM images of corresponding samples (see Section 3.4, Figs. 6–8). A broad band with the minimum at 580 cm^{-1} indicates the presence of only Fe_3O_4 as a single iron oxide phase [46,62,63], which tallies with the XRD and Mössbauer measurements.

3.4. FE-SEM and EDS

Reference sample G-2 h consists of uniform lath-like α-FeOOH particles 150–200 nm long, 40–60 nm wide and 10–20 nm thick (Fig. 1a). The presence of 1 mol% of Ir^{3+} ions in the precipitation system significantly changed the size of obtained particles. Larger α-(Fe,Ir)OOH lath-like particles were obtained with about 400–600 nm length, 60–80 nm width and 20–30 nm thickness (Fig. 6a and b). Similar α-(Fe,Ir)OOH particles were still present in the sample obtained after 6 h of hydrothermal treatment (Fig. 6c). These particles were partially transformed after 24 h of treatment to α-Fe_2O_3 crystals in the form of hexagonal bipyramids of about 1 μm length (Fig. 6d). EDS analysis showed no significant amount of iridium in these α-Fe_2O_3 crystals, which explains the presence of a weakly ferromagnetic order in this α-Fe_2O_3 (like in pure α-Fe_2O_3), as observed by Mössbauer spectroscopy (Fig. 2, Table 2). The α-(Fe,Ir)OOH → α-Fe_2O_3 transformation was almost completed after 72 h, but α-Fe_2O_3 crystals were further partially
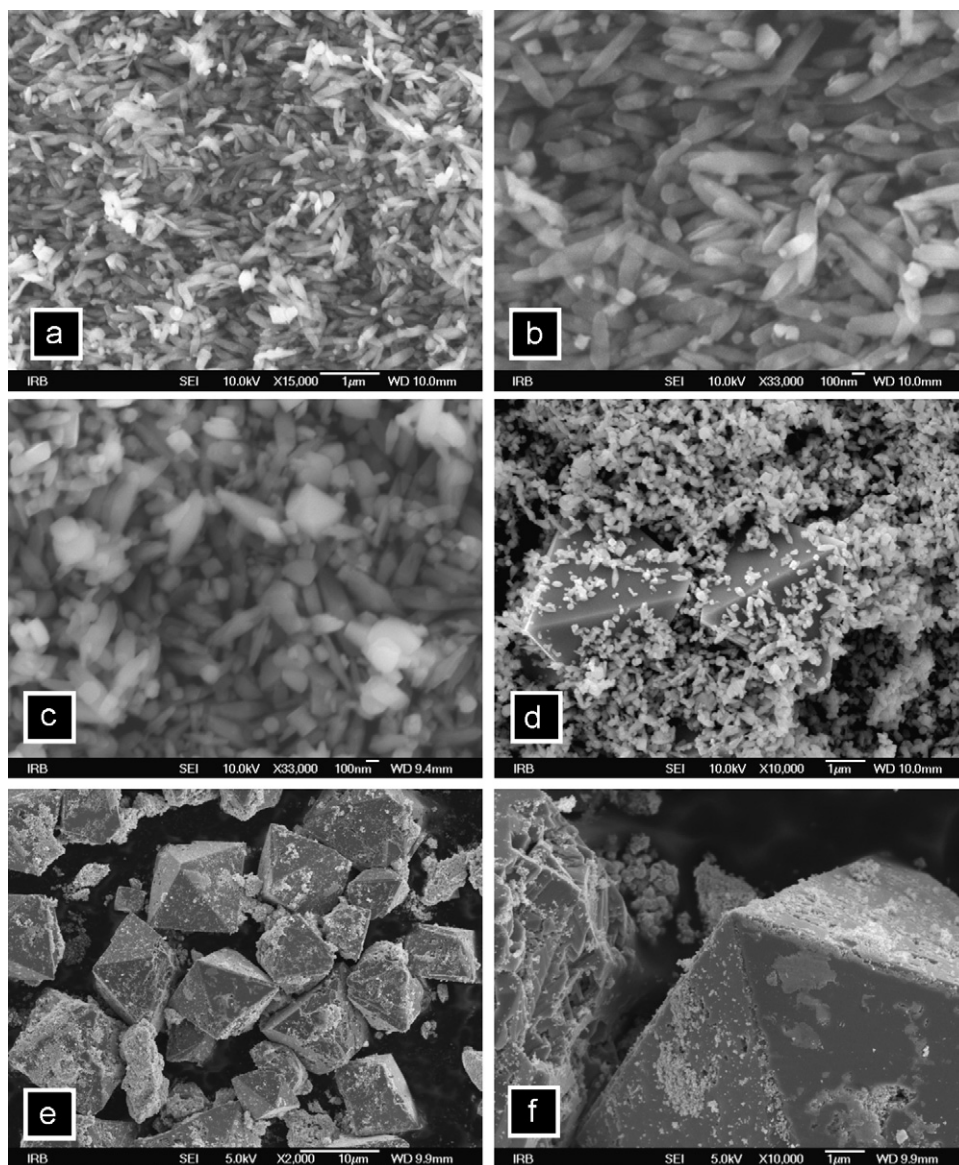
Fig. 7. FE-SEM images of samples: IrG5-2 h at lower (a) and higher (b) magnification, IrG5-6 h (c), IrG5-24 h (d), IrG5-72 h at lower (e) and higher (f) magnification.

transformed to large (about 10 μm dia) octahedral Fe_3O_4 crystals (Fig. 6e). A small quantity of elongated α-(Fe,Ir)OOH particles was still present at the surface of α-Fe_2O_3 crystals along with metallic iridium nanoparticles responsible for the catalytic reduction of Fe(III)–Fe(II) (Fig. 6f).

The presence of 5 mol% of Ir^{3+} ions in the precipitation system led to the formation of spindle-shaped α-(Fe,Ir)OOH particles (Fig. 7a and b) with 300–700 nm length and 100–200 nm width, along with a significant number of smaller (20–100 nm dia) α-(Fe,Ir)$_2O_3$ particles. A longer hydrothermal treatment (6 h) resulted in an increase in the number and size of α-(Fe,Ir)$_2O_3$ particles (Fig. 7c). These particles show significant differences in size and shape in comparison with bipyramidal α-Fe_2O_3 crystals obtained in the presence of 1 mol% of Ir^{3+} ions (Fig. 6d). EDS analysis showed about 2 mol% of iridium (in respect to overall metal content) in these α-Fe_2O_3 particles, which confirms the assumption that Ir-for-Fe substitution in hematite is the cause for a change in the magnetic order (at room temperature) from weakly ferromagnetic to antiferromagnetic. With further hydrothermal treatment (for 24 h) the α-(Fe,Ir)OOH and α-(Fe,Ir)$_2O_3$ particles partially transformed to octahedral Fe_3O_4 crystals (Fig. 7d). EDS analysis showed no significant amount of iridium in these crystals, i.e., no significant Ir-for-Fe substitution in the Fe_3O_4 structure. After 72 h of hydrothermal treatment the transformation was completed, resulting in the formation of large (5–10 μm in diameter) octahedral Fe_3O_4 crystals and small iridium nanoparticles (Fig. 7e and f).

The transformation α-(Fe,Ir)OOH → α-(Fe,Ir)$_2O_3$ → Fe_3O_4 + Ir^0, with a similar course as in the precipitation system with 5 mol% of Ir^{3+} ions, was also observed for samples obtained in the presence of 10 mol% of Ir^{3+} ions (Fig. 8). The α-(Fe,Ir)OOH and α-(Fe,Ir)$_2O_3$ particles in these samples were significantly smaller in comparison with samples obtained in the presence of 5 mol% of Ir^{3+} ions (Fig. 7). The EDS analysis of sample IrG10-2 h showed only 4.32 mol% of iridium in this sample (in comparison with 10 mol% in the initial reaction mixture), which indicates a partial loss of iridium during sample washing.
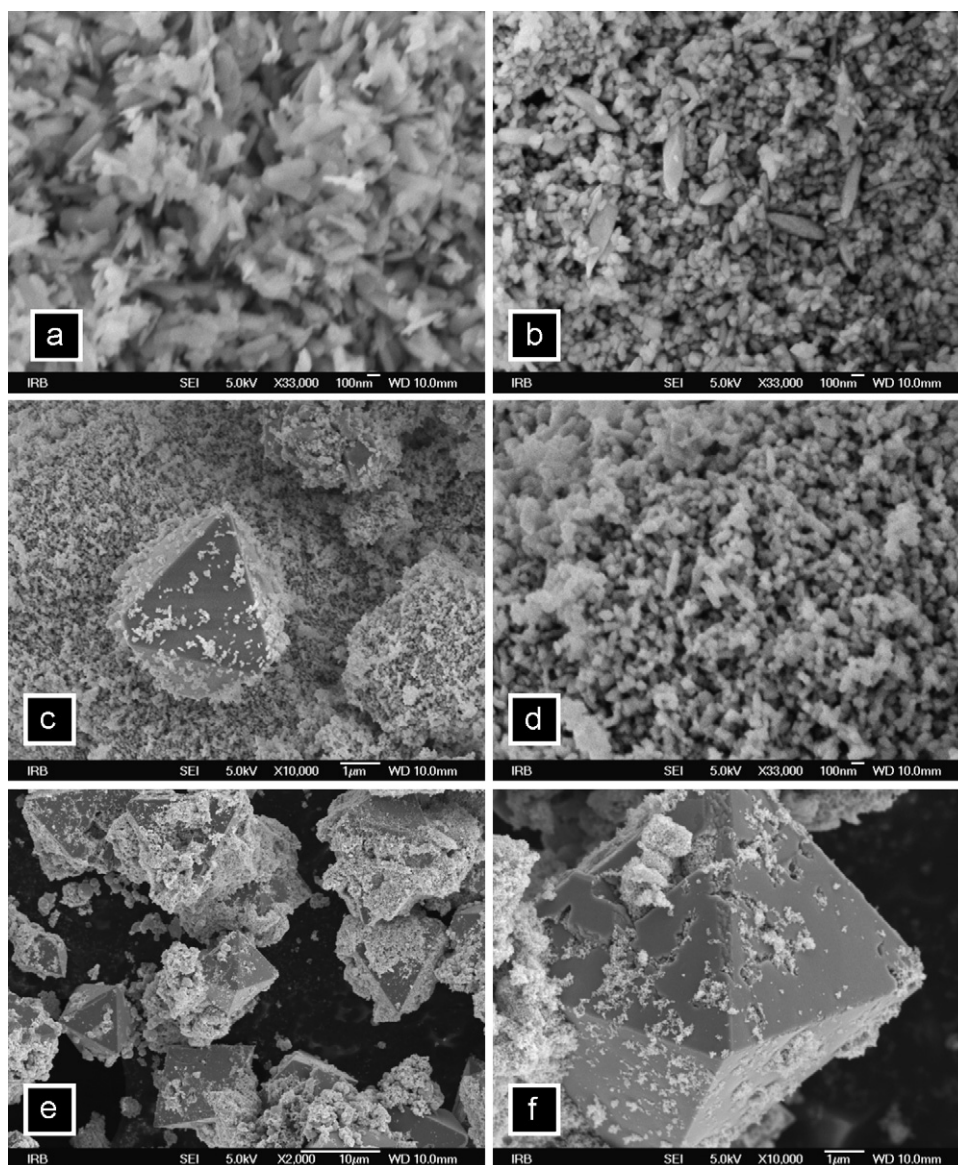
Fig. 8. FE-SEM images of samples: IrG10-2 h (a), IrG10-6 h (b), IrG10-24 h at lower (c) and higher (d) magnification, IrG10-72 h at lower (e) and higher (f) magnification.

4. Conclusions

- A strong influence exerted by the presence of iridium(III) ions on the phase composition, magnetic, structural and morphological properties of iron oxides formed in a highly alkaline medium in the presence of tetramethylammonium hydroxide was observed.
- The Ir^{3+}-for-Fe^{3+} substitution in the α-FeOOH structure induced changes in unit-cell dimensions, crystallite size, hyperfine magnetic field, structural vibrations, and the particle size and morphology.
- The Ir^{3+}-for-Fe^{3+} substitution in the α-Fe_2O_3 structure caused an increase in the temperature of the Morin transition - Mössbauer spectroscopy showed the presence of α-Fe_2O_3 in the antiferromagnetically ordered state at 293 K.
- A longer hydrothermal treatment of the precipitation systems in the presence of Ir^{3+} ions resulted in a gradual phase transformation α-(Fe,Ir)OOH $\rightarrow$ α-(Fe,Ir)$_2$O$_3$ $\rightarrow$ Fe$_3$O$_4$ + Ir^0.
- Iridium is both a reactant and a catalyst in this phase transformation.

References

[1] R.M. Cornell, U. Schwertmann, The Iron Oxides, Structure, Properties, Reactions, Occurrence and Uses, second ed., Wiley-VCH, 2003.
[2] M.P. Sharrock, R.E. Bodnar, J. Appl. Phys. 57 (1985) 3919–3924.
[3] P. Li, D.E. Miser, S. Rabiei, R.T. Yadav, M.R. Hajaligol, Appl. Catal. B 43 (2003) 151–162.
[4] Z. Lu, S.-H. Lee, S.V. Babu, E. Matijević, J. Colloid Interface Sci. 261 (2003) 55–64.
[5] P. Tartaj, M. del Puerto Morales, S. Veintemillas-Verdaguer, T. Gonzalez-Carreno, C.J. Serna, J. Phys. D: Appl. Phys. 36 (2003) R182–R197.
[6] M.A. Willard, L.K. Kurihara, E.E. Carpenter, S. Calvin, V.G. Harris, Int. Mater. Rev. 49 (2004) 125–170.
[7] W. Zhang, P. Singh, E. Paling, S. Delides, Miner. Eng. 17 (2004) 517–524.
[8] S. Laurent, D. Forge, M. Port, A. Roch, C. Robic, L. Vander Elst, R.N. Muller, Chem. Rev. 108 (2008) 2064–2110.
[9] Y. Kubota, H. Morita, Y. Tokuoka, Y. Imaoka, IEEE Trans. Magn. 15 (1979) 1558–1560.
[10] J.Z. Jiang, R. Lin, W. Lin, K. Nielsen, S. Mørup, K. Dam-Johansen, R. Clasen, J. Phys. D: Appl. Phys. 30 (1997) 1459–1467.
[11] M.A. Wells, R.W. Fitzpatrick, R.J. Gilkes, J. Dobson, Geophys. J. Int. 138 (1999) 571–580.
[12] O.K. Tan, W. Cao, Y. Hu, W. Zhu, Ceram. Int. 30 (2004) 1127–1133.
[13] M. Mohapatra, S.K. Sahoo, S. Anand, R.P. Das, J. Colloid Interf. Sci. 298 (2006) 6–12.

[14] Y. Wang, F. Kong, B. Zhu, S. Wang, S. Wu, W. Huang, Mater. Sci. Eng. B 140 (2007) 98–102.
[15] I.R. Guimaraes, A. Giroto, L.C.A. Oliveira, M.C. Guerreiro, D.Q. Lima, J.D. Fabris, Appl. Catal. B: Environ. 91 (2009) 581–586.
[16] U. Schwertmann, R.M. Cornell, Iron Oxides in the Laboratory, Preparation and Characterization, second ed., Wiley-VCH, 2000.
[17] S. Krehula, S. Musić, S. Popović, J. Alloys Compd. 403 (2005) 368–375.
[18] S. Krehula, S. Musić, J. Alloys Compd. 416 (2006) 284–290.
[19] S. Krehula, S. Musić, J. Alloys Compd. 426 (2006) 327–334.
[20] S. Krehula, S. Musić, Mater. Chem. Phys. 123 (2010) 67–76.
[21] J.Z. Liu, J. Magn. Magn. Mater. 54–57 (1986) 901–902.
[22] A. Punnoose, T. Phanthavady, M.S. Seehra, N. Shah, G.P. Huffman, Phys. Rev. B 69 (2004) 054425.
[23] F.J. Berry, X. Changhai, S. Jobson, J. Chem. Soc. Faraday Trans. 86 (1990) 165–169.
[24] F.J. Berry, S. Jobson, Hyperfine Interact. 69 (1991) 775–778.
[25] W. Zhang, Y. Huang, J. Wang, K. Liu, X. Wang, A. Wang, T. Zhang, Int. J. Hydrogen Energy 35 (2010) 3065–3071.
[26] S.D. Tilley, M. Cornuz, K. Sivula, M. Grätzel, Angew. Chem. Int. Ed. 49 (2010) 6405–6408.
[27] S. Krehula, S. Popović, S. Musić, Mater. Lett. 54 (2002) 108–113.
[28] S. Krehula, S. Musić, J. Cryst. Growth 310 (2008) 513–520.
[29] http://www.ccp14.ac.uk/ccp/web-mirrors/llnlrupp/weblat/weblat.htm, XLAT (A Least Squares Microcomputer Program for the Refinement of Cell Constants).
[30] Govaert, C. Dauwe, P. Plinke, E. De Grave, J. De Sitter, J. Phys. Colloques 37 (1976) C6825–C6827.
[31] F.J. Morin, Phys. Rev. 78 (1950) 819–820.
[32] D. Schroeer, R.C. Nininger, Phys. Rev. Lett. 19 (1967) 632–634.
[33] E. Murad, J.H. Johnston, Iron oxides and oxyhydroxides, in: G.J. Long (Ed.), Mössbauer Spectroscopy Applied to Inorganic Chemistry, vol. 2, Plenum Publishing Corporation, 1987, p. 507.
[34] A.H. Morrish, Canted Antiferromagnetism: Hematite, World Scientific Publishing Co., Singapore, 1994.
[35] P.J. Besser, A.H. Morrish, C.V. Searle, Phys. Rev. 153 (1967) 632–640.
[36] E. De Grave, D. Chambaere, L.H. Bowen, J. Magn. Magn. Mater. 30 (1983) 349–354.
[37] R.E. Vandenberghe, A.E. Verbeeck, E. De Grave, W. Stiers, Hyperfine Interact. 29 (1986) 1157–1160.
[38] Ayub, F.J. Berry, R.L. Bilsborrow, Ö. Helgason, R.C. Mercader, E.A. Moore, S.J. Stewart, P.G. Wynn, J. Solid State Chem. 156 (2001) 408–414.
[39] G.M. da Costa, E. Van San, E. De Grave, R.E. Vandenberghe, V. Barrón, L. Datas, Phys. Chem. Miner. 29 (2002) 122–131.
[40] E.E. Sileo, D.P. Daroca, Barrero, Larralde, Giberti, Saragovi, Chem. Geol. 238 (2007) 84–93.
[41] J.M.D. Coey, G.A. Sawatzky, J. Phys. C: Solid State Phys. 4 (1971) 2386–2407.
[42] J.Z. Liu, C.L. Fan, Phys. Lett. 105A (1984) 80–82.
[43] Ö. Helgason, I. Ayub, F.J. Berry, E. Crabb, Hyperfine Interact. 141/142 (2002) 291–295.
[44] I. Tanczos, Gy. Pokol, J. Borsa, T. Tóth, H. Schmidt, J. Anal. Appl. Pyrolysis 68–69 (2003) 173–185.
[45] S. Krehula, S. Musić, Croat. Chem. Acta 84 (2011) 465–468.
[46] S. Krehula, S. Musić, Croat. Chem. Acta 80 (2007) 517–527.
[47] S. Krehula, S. Musić, J. Mol. Struct. 924–926 (2009) 201–207.
[48] S. Krehula, S. Musić, J. Mol. Struct. 976 (2010) 61–68.
[49] S. Krehula, S. Musić, J. Mol. Struct. 993 (2011) 382–389.
[50] J. Gerth, Geochim. Cosmochim. Acta 54 (1990) 363–371.
[51] W. Stiers, U. Schwertmann, Geochim. Cosmochim. Acta 49 (1985) 1909–1911.
[52] A.C. Scheinost, H. Stanjek, D.G. Schulze, U. Gasser, D.L. Sparks, Amer. Miner. 86 (2001) 139–146.
[53] E.E. Sileo, M. Alvarez, E.H. Rueda, Int. J. Inorg. Mater. 3 (2001) 271–279.
[54] L. Verdonck, S. Hoste, F.F. Roelandt, G.P. van der Kelen, J. Mol. Struct. 79 (1982) 273–279.
[55] P. Cambier, Clay Miner. 21 (1986) 191–200.
[56] P. Cambier, Clay Miner. 21 (1986) 201–210.
[57] U. Schwertmann, P. Cambier, E. Murad, Clays Clay Miner. 33 (1985) 369–378.
[58] C.J. Serna, J.L. Rendon, J.E. Iglesias, Spectrochim. Acta 38A (1982) 797–802.
[59] Y. Wang, A. Muramatsu, T. Sugimoto, Colloid Surf. A: Phys. Eng. Aspects 134 (1998) 281–297.
[60] S. Krehula, S. Musić, J. Alloys Compd. 431 (2007) 56–64.
[61] S. Krehula, S. Musić, J. Mol. Struct. 834–836 (2007) 154–161.
[62] N.T. McDevitt, W.L. Baun, Spectrochim. Acta 20 (1964) 799–808.
[63] M. Gotić, G. Koščec, S. Musić, J. Mol. Struct. 924–926 (2009) 347–354.